Design, Modeling, and Validation of an Extendable Tendon-Driven Robot for Long-Term Deployment in Congested and Evolving Outdoor Environments

Nolan Howard[1], Ziyang Zhou[2], Suyi Li[2], and Ian D. Walker[1]
[1]Department of Electrical Engineering and Computer Science,
University of Wyoming, Laramie, WY 82071 USA
[2] Department of Mechanical Engineering, Virginia Polytechnic Institute, Blacksburg, VA 24061 USA
nhoward3@uwyo.edu, zzhou4@vt.edu, suyili@vt.edu, iwalker2@uwyo.edu

***Abstract*— Robotic systems for long-term monitoring in dense natural environments require a minimal physical footprint with the ability to maneuver through confined spaces, while being robust to harsh conditions. This work presents the design, modeling, and implementation of a compact, tendon-driven continuum robot capable of controlled extension and spatial bending within a self-contained, protective actuation package. The system is comprised of a meter-long, single-section, three-tendon "tendril" that deploys from a central reel mechanism. Integrated load cells provide tension sensing, and a tip camera supports control feedback and data collection. A Denavit-Hartenberg-based kinematic model is adapted to enable motion planning for the variable-length continuum section. To compensate for modeling inaccuracies arising from the inherent compliance of the flexible tendril, a closed-form tension distribution model is introduced to support feedback-based refinement of the robot pose. The robot prototype demonstrated navigating cluttered natural environments and was deployed outdoors over a total of five months, exhibiting resiliency to extreme environmental conditions.**

I. Introduction

This paper introduces a novel, compact continuum robot tendril prototype capable of both extension/retraction and variable section length bending (Fig. 1). The overarching goal of the research is to explore how robotic systems can emulate plant behaviors such as slow, deliberate movement, environmental responsiveness, and morphological adaptation to efficiently interact with and monitor complex ecosystems over extended durations. Within this concept, the extendable continuum robot plays a role analogous to plant vines: as a deployable, self-contained "tendril" capable of long-term deployment in, and navigation of, the confined environments that will be found where it is deployed.

Specifically, our research focuses on monitoring and responding to both *long-term processes* (e.g., pollution spread, humidity levels, seasonal migration of animal groups) and *related but randomly occurring real-time events* (e.g., pollution outbreaks, forest fires, sightings of rare animals). Moreover, these long-term and real-time events often occur in congested environments that evolve slowly but substantially over time (e.g., outdoor spaces with propagating vegetation). The requirements to operate with these multiple time scales and in congested, time-varying environments preclude the deployment of drones or other traditional mobile robots.



Fig. 1. Robot during one of its deployments outdoors on a roof.

We believe that a most promising approach for addressing the unique challenges above is to enable robots to behave somewhat like plants. Plants inherently possess capabilities inspirational for robotic operation in long-duration monitoring in dynamically evolving environments - enduring presence over months, decades, or even centuries; expanding and adapting their structure in response to environmental conditions [1], [2], [3], [4], [5]. However, plants grow by continuously converting materials from their surroundings, a process that would be structurally and energetically challenging for robotics.

Therefore, rather than directly copying the physiological mechanisms in plants, we are focusing on innovative structural and operational strategies to enable plant-like behaviors relevant to the envisioned monitoring missions. Specifically, we are exploring continuum robot "tendrils".

Continuum robots differ fundamentally from traditional rigid-link robots by offering compliant, continuously deformable backbones [6], [7], [8]. Their intrinsic compliance makes them particularly useful for tasks involving interaction with a delicate environment or traversal through unstructured spaces. The design of many continuum robots draws direct inspiration from natural systems such as elephant trunks [9], octopus arms [10], [11], snakes [12], and vines [13], [14]. Collectively, research over the past 20 years has demonstrated that continuum systems are capable of performing a variety of robotic tasks without relying on rigid skeletal

structures.

Among continuum designs, tendon-driven robots are especially common due to their inexpensive design and simplicity in controlling constant curvatures through applied tension [15]. Despite their simplicity, tendon-driven robots often have bulky actuation packages at the base [16], [17], [18]. Additionally, these systems typically rely on fixed-length backbone sections. When extension is required for this type of robot, this is typically achieved with space-inefficient linear actuators mounted at the base, increasing the overall system size and reducing its adaptability in tight environments [9], [19]. Some tendon-driven robots have been developed with clever extension mechanisms, however, they are either overly compliant [20] or exposed [21], [22], [23]. Furthermore, maintaining consistent tendon tension is often difficult, especially during dynamic movement, leading to slack, reduced accuracy, and control instability.

The robot introduced in this work builds on the established principles of creating tendon-driven robots, e.g. [16], [24], [25], [26], [27], [28], [29] but features a novel, compact design capable of both bending and extension. The robot is able to dynamically adjust its arc length during operation and has a very high length-diameter ratio in the fully extended state. The extension reel developed for this robot enables use of a simple kinematics model and has proven resilient in long-term outdoor deployment. The compact design is enhanced with integrated tension sensing, enabling more accurate and stable tendon control.

The tendril design and its realization are described in the following section. Modeling of the system is discussed in section III. Experiments with the robot, aimed at enabling long-term monitoring and exploration in outdoor environments that require minimal footprint and high maneuverability, are reported in section IV. Conclusions are presented in section V.

II. Mechanical Design and Control

The mechanical design of the continuum robot focuses on achieving compactness and mechanical simplicity while enabling both bending and extension/retraction capabilities. The structure is engineered to extend and retract smoothly from a central reel and bend via tendon actuation. The robot's architecture prioritizes self-containment, minimizing the footprint of actuation systems to enable deployment in constrained environments.

A. Tendril

The robot consists of a single section, tendon-driven continuum arm referred to as the "tendril" illustrated in Fig. 2. A classical three-tendon continuum robot design, with the tendons spaced 120 degrees apart radially about the backbone, is implemented. Friction in the tendril is meticulously minimized throughout design iterations. The final prototype uses nylon-coated tendon materials and low-friction plastic material for the spacers, and includes roller bearings where the tendons make sharp curves in their routing to the actuators. The spacers are shaped with a chamfer on the bottom to prevent jams when the tendril is retracting into the reel. Additionally, there is an endoscope camera at the tip (Enable Imaging minnieScope-XS), with the cable routed through holes in the spacers. The camera cable is routed adjacent to the backbone to minimize stretching or compressing of the cable as the tendril curves.

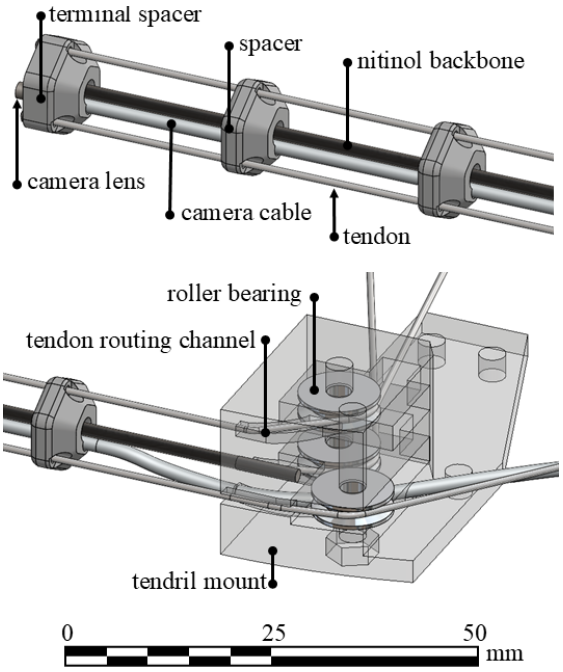


Fig. 2. Tendril design details.

B. Extension Mechanism

The base of the tendril is mounted to a cylindrical spool that acts as the extension reel. The extension of the robot is controlled by unwinding the flexible tendril from the coil, increasing the arc length of the robot. This robot introduced two novel mechanisms in the reel. First, the spool has a hex-grooved channel corresponding to the tendril's hex-shaped spacers. This prevents torsion within the housing to improve conformance with the kinematics model. Secondly, the extension reel uses a funnel tangent to the tendril coil to guide the tendril to a defined exit position and direction. This simplifies the kinematics because the origin of the tendril is fixed at the funnel tip with a vertical orientation. Details of the design of the reel are shown in Fig. 3.

TABLE I
Design Specifications - Dimensions

Parameter	Dimension
Total tendril length	1000 mm
Extendable tendril length	811 mm
Spool diameter	179 mm
Spacer linear spacing	25 mm
Spacer diameter	10 mm
Tendon radial spacing	4.8 mm
Backbone diameter	1.5 mm
Tendon cable diameter	0.6 mm

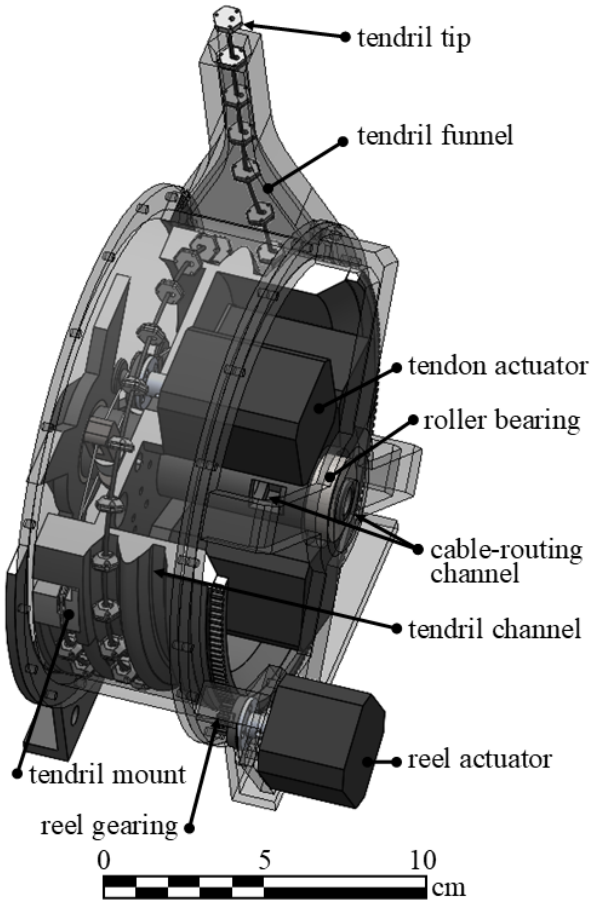


Fig. 3. Partial cross section of reel mechanism.

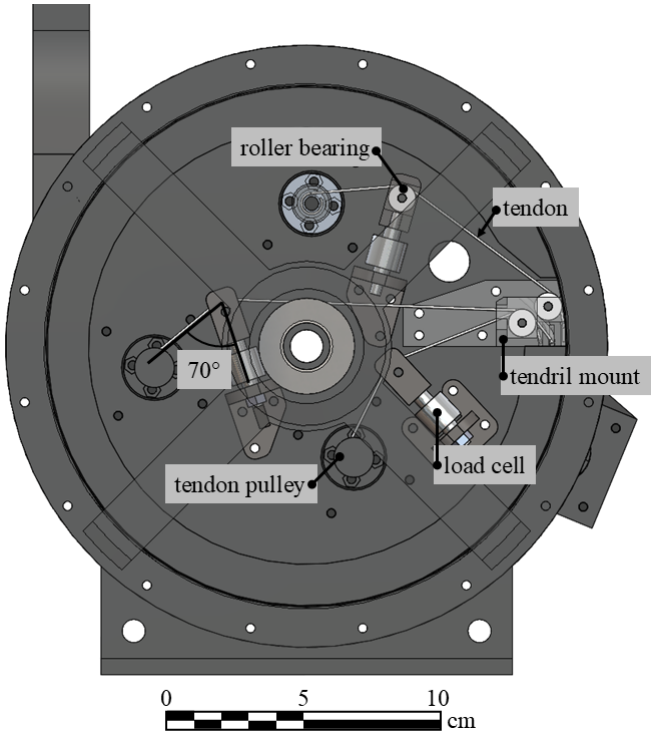


Fig. 4. Tendon routing detail.

TABLE II
DESIGN SPECIFICATIONS - MATERIALS

Component	Material
Backbone	Nitinol
Spacers	3D printed with iglide® tribo-filament
Backbone-to-spacer adhesive	*J-B Weld* 2-part epoxy
Reel mechanism	3D printed with PETG
Tendons	Nylon-coated braided stainless steel

C. Actuation

The three tendons are individually actuated by stepper motors (NEMA 17 bipolar 1.8 degree) to control curvature. A fourth motor of the same type drives the extension via the geared rotation of the reel. The tendon motors are mounted on the inner spool of the reel mechanism. The cables are routed from the tendril base mount to a small pulley mounted directly on the motor shaft which winds the tendons, changing their length. Tension is monitored using load cells (DYMH-113) located between the base of the tendril and the tendon pulleys to provide control feedback. The routing of the tendons from the tendril, across the load cells, and to the motors is shown in Fig. 4.

D. Control

The control architecture for the continuum robot integrates high-level planning in MATLAB with real-time actuation and

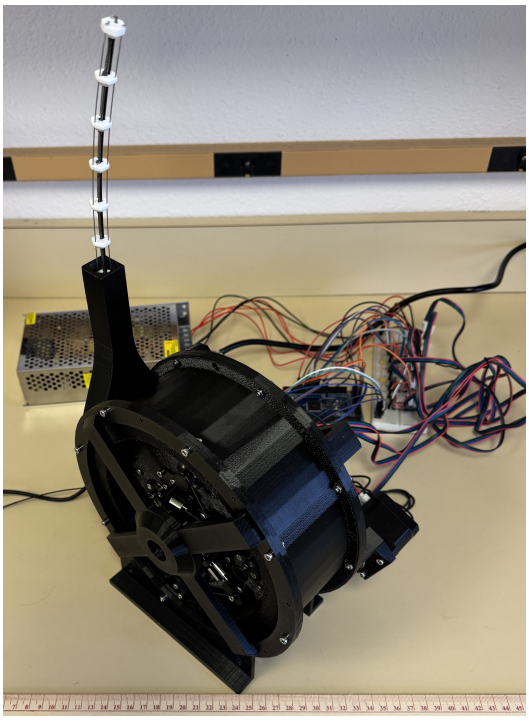


Fig. 5. Robot and external electronics. External connections are power to 120 VAC and Arduino and Camera USB to PC.

sensing via an Arduino MEGA 2560 microcontroller. MATLAB serves as the central interface for computing inverse kinematics, executing motion sequences, and coordinating sensor data. It communicates with the Arduino to send target motor positions.

Low-level control from the Arduino drives the four stepper motors via A4988 motor driver boards. Tendon tension is monitored by three load cells. The signal from the load cells provides digital force measurements to the Arduino via HX711 ADC amplifier boards.

In addition to low level control, MATLAB receives images from the tip camera via a USB video processing unit, enabling visual feedback in addition to data collection. This control framework allows for easy integration with high-level MATLAB processing of kinematics and camera feedback. A block diagram representing the software and hardware connections of the control system is provided in Fig. 6.

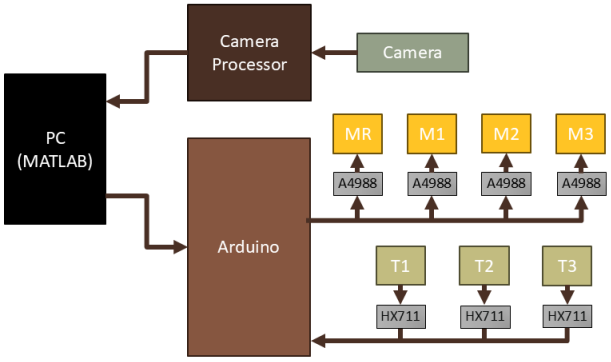


Fig. 6. Control system block diagram. MR reel stepper motor and M1-M3 tendon actuators controlled by A4988 drivers. T1-T3 tension load cells amplified by HX711 ADCs.

III. Kinematic Modeling

Modeling the kinematics of continuum robots presents unique challenges compared to traditional rigid-link systems, due to their continuous structure with theoretically infinite degrees of freedom [30]. To address this, we adopt the modified Denavit–Hartenberg (DH) approach as introduced in [9]. This offers a practical framework for representing 3D constant-curvature continuum sections using the traditional kinematic techniques of Denavit-Hartenberg. The approach in [9], modified herein, converts discrete joint variables/rigid link lengths to a constant-curvature section using three continuous parameters: arc length s, curvature k, and bending plane angle ϕ. The section is modeled with the origin being at the tip of the funnel where the tendril exits the reel as shown in Fig. 7.

A key feature of this robot is that the section's arc length s is variable during operation, as is the number of spacer segments n used in the tendon-length calculations. Additionally, as the robot extends or retracts, the length of the tendril within the reel changes, which must be accounted for to obtain accurate tendon lengths. This is handled by modeling a secondary continuum section for the spooled tendril with a constant curvature k_{spool} and plane angle ϕ_{spool} but with a length s_{spool} that inversely relates to s. Desired tendon lengths are then the sum of lengths calculated in both sections.

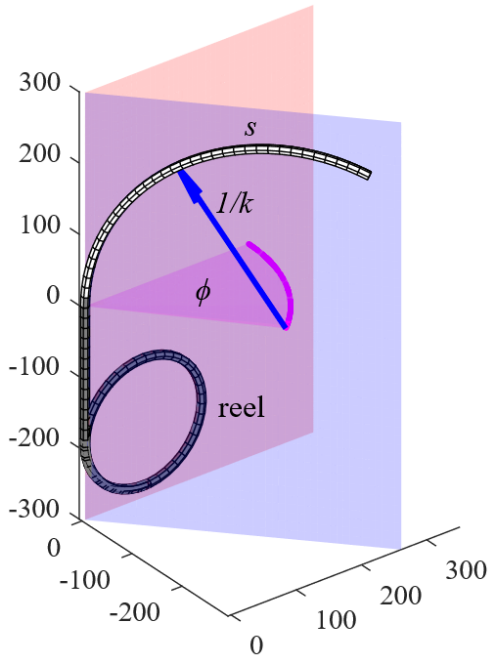


Fig. 7. Continuum parameters for tendril with reel.

A. Forward Kinematics

In the adapted DH method, the single continuum section is initially represented as a virtual 4-axis rigid-link robot with a revolute–revolute–prismatic–revolute architecture [9]. The elements of the resulting homogeneous transformation matrix for the virtual robot are transformed via basic constant curvature geometry [9] to the continuum robot representation in terms of shape variables $\underline{q} = \begin{bmatrix} s & k & \phi \end{bmatrix}^T$. This is expressed in (1). The translational vector in the top-right corner of this matrix, $\underline{x} = \begin{bmatrix} x & y & z \end{bmatrix}^T$, gives tip position relative to the base frame and is used for forward position kinematics.

B. Inverse Kinematics

Again using the approach from [9], the Jacobian in (2) is derived for velocity kinematics. The inverse kinematics of the robot is then solved by iteratively solving velocity kinematics. This Jacobian-based method proved effective for our robot.

In more detail, given a desired position $\underline{x}_d = \begin{bmatrix} x_d & y_d & z_d \end{bmatrix}^T$, the algorithm iteratively updates shape variables $\underline{q}$ to move the tip to the target. At each iteration, the current tip position $\underline{x}$ is computed from the forward kinematics matrix $[\mathbf{H}]$. The linear velocity $\underline{\dot{x}}$ required to move toward the desired position is approximated as the difference vector $\underline{x}_d - \underline{x}$. To solve for joint velocities from linear velocities the inverse of the Jacobian is used:

$$\underline{\dot{q}} = \mathbf{J^{-1}}\underline{\dot{x}} \tag{3}$$

$$[\mathbf{H}] = \begin{bmatrix} \cos\phi\cos ks & -\sin\phi & -\cos\phi\sin ks & -\frac{1}{k}(\cos\phi - \cos\phi\cos ks) \\ \sin\phi\cos ks & \cos\phi & -\sin\phi\sin ks & -\frac{1}{k}(\sin\phi - \sin\phi\cos ks) \\ \sin ks & 0 & \cos ks & \frac{1}{k}\sin ks \\ 0 & 0 & 0 & 1 \end{bmatrix} \tag{1}$$

$$[\mathbf{J}] = \begin{bmatrix} -\sin ks\cos\phi & \frac{1}{k^2}(\cos\phi(1-\cos ks - ks\sin ks)) & \frac{1}{k}((1-\cos ks)\sin\phi) \\ -\sin ks\sin\phi & \frac{1}{k^2}(\sin\phi(1-\cos ks - ks\sin ks)) & -\frac{1}{k}((1-\cos ks)\cos\phi) \\ \cos ks & -\frac{1}{k^2}(\sin ks - ks\cos ks) & 0 \end{bmatrix} \tag{2}$$

A small time step Δt is used to update the shape variables:

$$\underline{q}_{next} = \underline{q}_{current} + \Delta t \cdot \dot{\underline{q}} \tag{4}$$

After the desired shape variables $\underline{q}$ are found, tendon lengths are derived using (5–7) from [31], where d is the radial distance of the tendons from the centerline and n is the number of spacer segments which are set according to the robot's corresponding parameters. Here, n is treated as a variable dependent on s and the segment spacing of 25 mm.

$$l_1 = 2n\sin\left(\frac{ks}{2n}\right)\left(\frac{1}{k} + d\sin\phi\right) \tag{5}$$

$$l_2 = 2n\sin\left(\frac{ks}{2n}\right)\left(\frac{1}{k} + d\sin\left(\frac{2\pi}{3} + \phi\right)\right) \tag{6}$$

$$l_3 = 2n\sin\left(\frac{ks}{2n}\right)\left(\frac{1}{k} + d\sin\left(\frac{4\pi}{3} + \phi\right)\right) \tag{7}$$

$$d = 4.8 \tag{8}$$

$$n = \frac{s}{25} \tag{9}$$

It is not sufficient to only calculate tendon lengths for the portion of the robot outside the housing because as the tendril extends, the amount of curvature inside the reel is changing. To account for the curvature of the robot around the spool, a second continuum section is considered where the tendon length equations (5–7) are used with the values for the joint variables defined as:

$$s_{spool} = s_{total} - s_{funnel} - s = 1000 - 189 - s \tag{10}$$

$$k_{spool} = \frac{1}{r_{spool}} = \frac{1}{89.5} \tag{11}$$

$$\phi_{spool} = \pi \tag{12}$$

Total tendon lengths are found by summing the lengths inside and outside the spool. Tendon lengths are converted to motor positions linearly by relating to the circumference of the tendon pulleys. The motor position for the extension motor is linearly related to s through gear ratio $188:12$.

A test was performed with this model in which the robot was commanded to move to several different tip positions sequentially. The actual tip positions were roughly measured by hand using a ruler. The results of that test are shown in Table III.

TABLE III
EXPERIMENTAL RESULTS

Commanded Position [mm]	Measured Position [mm]	s [mm]	Error [mm]	Error [%]
$(50, 0, 200)$	$(40, 0, 200)$	208	10	4.8
$(-100, 0, 200)$	$(-40, 0, 230)$	232	67	28.9
$(0, 100, 250)$	$(0, 40, 275)$	276	65	23.6
$(0, 200, 250)$	$(0, 80, 335)$	346	147	42.5
$(0, -200, 250)$	$(0, -80, 335)$	346	147	42.5
$(200, -200, 300)$	$(180, 100, 380)$	454	311	68.5
$(-200, 200, 300)$	$(-240, 175, 300)$	454	47	10.4
$(-100, -100, 500)$	$(-140, -30, 500)$	526	81	15.4
$(-100, 100, 100)$	$(-100, 90, 140)$	203	41	20.2
$(0, 0, 50)$	$(0, 0, 50)$	50	0	0.0
$(0, 0, 250)$	$(20, 0, 250)$	250	20	8.0
$(0, 0, 500)$	$(-10, 50, 500)$	500	51	10.2
$(0, 0, 1000)$	$(-880, 80, 240)$	1000	1166	116.6
$(-150, -150, 400)$	$(-130, -60, 450)$	471	105	22.3
$(-150, 150, 250)$	$(-150, -40, 320)$	357	130	36.4
$(100, 25, 250)$	$(60, 20, 270)$	277	45	16.2

The experimental results demonstrate that the kinematics model enables the robot to move in the correct general direction to commanded positions. However, as the tendril extended further, the accuracy degrades significantly. This was most evident in trials with long extensions where the measured error exceeded 1 meter. In this case, the extreme length of the tendril was affected by gravity and the robot "tipped over" due to its flexibility and lack of supports. The errors in position accuracy can be explained by accumulated tendon friction, increased slack, and reduced mechanical stiffness as more of the backbone leaves the spool.

Despite these limitations, the inverse kinematics algorithm reliably generated joint trajectories that resulted in smooth motion, and the actual tendril lengths achieved by the extension motor were very accurate. Therefore this model provided a foundation for motion which could be supplemented with additional feedback.

C. Tension Distribution Model

The constant-curvature kinematic model does not account for friction, gravity, or material compliance. Therefore, at a fixed extension length, measured tendon tensions can be used to refine the robot pose after an inverse-kinematics command is used. Each tendon produces a bending moment about the backbone, and the combined effect of the three tendon tensions determines the magnitude and direction of the resulting bend. The three tendon tensions are represented by an equivalent planar bending resultant with magnitude T_c and direction ϕ. This mapping from three tensions spaced 120°

apart to a two-dimensional planar vector is mathematically equivalent to a Clarke transformation [32].

The desired bending effect is specified by the resultant magnitude T_c and direction ϕ. The corresponding tendon tensions are then obtained from the following closed-form distribution, which ensures nonnegative tension commands over the full range of bending directions.

Define the Cartesian components of the desired tension resultant as $v_x = T_c \cos\phi$ and $v_y = T_c \sin\phi$. The resulting closed-form tension distribution is:

$$\begin{cases} T_1 = \mathbf{v}_x + \dfrac{\mathbf{v}_y}{\sqrt{3}}, \\ T_2 = \dfrac{2\mathbf{v}_y}{\sqrt{3}}, \\ T_3 = 0, & 0^\circ < \phi < 120^\circ \\ \\ T_1 = 0, \\ T_2 = -\mathbf{v}_x + \dfrac{\mathbf{v}_y}{\sqrt{3}}, \\ T_3 = -\mathbf{v}_x - \dfrac{\mathbf{v}_y}{\sqrt{3}}, & 120^\circ < \phi < 240^\circ \\ \\ T_1 = \mathbf{v}_x - \dfrac{\mathbf{v}_y}{\sqrt{3}}, \\ T_2 = 0, \\ T_3 = -\dfrac{2\mathbf{v}_y}{\sqrt{3}}, & 240^\circ < \phi < 360^\circ \end{cases} \tag{13}$$

At $\phi = 0^\circ$, 120°, and 240°, the limiting solution applies, with only the corresponding tendon tensioned to T_c. This closed-form distribution provides intuitive tension commands for a desired bending direction and can be compared with load-cell measurements to refine the commanded pose in the presence of unmodeled effects.

IV. Outdoor Experiments

The ultimate goal for this robot is to mimic aspects of the behavior of plants to perform long-term environmental monitoring. Therefore, the next stage of the research was to demonstrate the ability to deploy this robot outdoors in sustained real environmental conditions. The robot was deployed in two different locations, first for testing and evaluation in an easily accessible location, then in a more environmentally interesting location for a longer (multi-month) duration.

A. Preliminary Deployment on Roof

The initial deployment was on the railing of a roof overlooking one of the Engineering buildings on campus (Fig. 8). The robot and electronics (including a mini-PC) were waterproofed inside sealed PETG 3D printed enclosures with cable glands, shrouded cooling fans, and a TPU gasket around the reel exit hole. The system was equipped with wireless access to allow remote monitoring and software changes without opening the enclosure. In this configuration, the base of the system was oriented so that the tendril emerged horizontally to enable monitoring of adjacent areas of interest in the retracted state.



Fig. 8. Tendril robot in waterproof box with electronics enclosure mounted on outdoor roof railing.

The preliminary deployment lasted for 8 weeks during which the system endured hailstorms, snow, and strong winds. During this time, the tendril extended at noon each day, moving through a series of preprogrammed positions to capture images of the entire area, then retracted to rest in the protective enclosure. Each deployment took 2–3 minutes to complete. In addition, a simple motion detection algorithm automatically took snapshots of interesting scenes throughout the experiment. Fig. 9 shows some images captured by the robot during its deployment.



Fig. 9. Images captured from initial outdoor deployment.

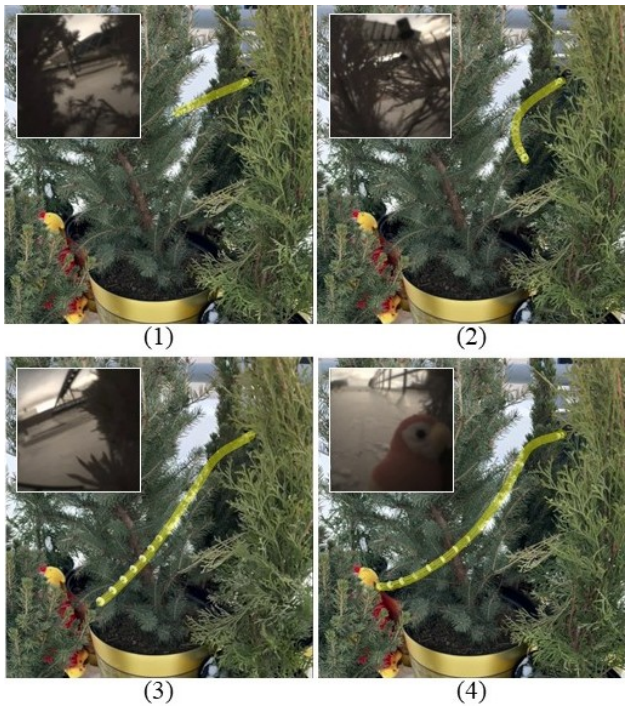


Fig. 10. Robot deploying in sequence (1) to (4), navigating simulated natural environment (tendril highlighted).

B. Confined Environment Demonstrations on Roof

During the multi-week deployment on the roof, experiments were conducted to showcase the capability of the robot to navigate a confined, natural environment. A semi-natural environment consisting of potted spruce trees was constructed next to the robot which was reoriented to face the plants. For these experiments, the robot was teleoperated, navigating through the plants to position the camera to look at the target toy bird. Several tests were conducted with varying plant positions, to demonstrate the ability of the robot to perform in an environment which may change over an extended deployment. Fig. 10 and the video submitted with the paper show the movements necessary to maneuver among the plants to locate the target in one of the experiments.

C. Extended Deployment on Lamppost

After successful tests on the roof, the robot was moved to a new location on campus to serve a role in a community vulture watch program which monitors Turkey Vulture population throughout the season. The robot was mounted on the top of a lamppost within view of the birds' seasonal nesting sites. A mounting adapter and electrical power were added to the top of the lamppost and the robot was deployed as shown in Fig. 11 in an updated waterproof enclosure.

At the time of submission, the robot has been deployed outdoors for a total of 5 months. During that time the robot has withstood a temperature range of $-25°C$ – $20°C$, wind speeds up to 95 km/h, and a total of 75 mm of precipitation including rain, hail, and snow (Fig. 12). The robot has successfully deployed more than 100 times, extending to lengths up to 800 mm, achieving bending radii as small as 50 mm, and experiencing tensions up to 60 N, without any significant mechanical failures during autonomous operation.



Fig. 11. Robot deployed on top of lamppost with view of nearby Turkey Vulture nesting site.



Fig. 12. Robot operated in harsh natural conditions.

V. Conclusions and Future Work

This work presented the design, modeling, and testing of a novel compact, tendon-driven extendable continuum robot for extended outdoor deployment. A conceptually complex design that includes extension, retraction, and spatial curvature control with tension sensing was implemented and packaged in a clean, compact, and mechanically simple prototype. The robot is capable of smooth extension and directional control using a Jacobian-based kinematics algorithm supplemented with a closed-form tension model. Experiments with the robot deployed outdoors over 5 months demonstrate the robot in sustained winter conditions and its ability to navigate a complex, constrained environment, validating its intended role as a means of long-term sensing in natural environments. These initial results establish a

strong foundation for further development toward application in increasingly challenging environments.

The robot will continue its deployment capturing images of Turkey Vultures as they migrate to and from the nesting site within view. Future development will focus on enabling autonomous operation by integrating vision-based feedback from the tip-mounted camera. This capability will allow the continuum robot to transition from manual point-to-point operation to an intelligent, perception-driven system. As a part of our larger plant-inspired research objective, the robot will be combined with a rigid "trunk" structure through which it will navigate, expanding the robot workspace. These enhancements will support a broader vision of using plant-inspired robotic systems for long-term, adaptive environmental monitoring in complex, dynamic environments.

VI. Acknowledgments

This work was supported in part by NSF grants 2506466 and 2312422.

References

[1] B. Mazzolai, L. Beccai, and V. Mattoli, "Plants as model in biomimetics and biorobotics: new perspectives," *Frontiers in Bioengineering and Biotechnology*, pp. 1–5, Jan. 2014.

[2] E. D. Dottore, A. Sadeghi, A. Mondini, and B. Mazzolai, "Continuous growth in plant-inspired robots through 3d additive manufacturing," in *2018 IEEE International Conference of Robotics and Automation (ICRA)*, 2018, pp. 3454–3460.

[3] F. Putzu, T. Abrar, and K. Althoefer, "Plant-inspired soft pneumatic eversion robot," in *2018 IEEE International Conference on Biomedical Robotics and Biomechatronics*, 2018, pp. 1327–1332.

[4] A. Sadeghi, A. Tonazzini, L. Popova, and B. Mazzolai, "Robotic mechanism for soil penetration inspired by plant root," in *2013 IEEE International Conference on Robotics and Automation (ICRA)*, 2013, pp. 3457–3462.

[5] N. Truong-Thinh and N. Ngoc-Phuong, "Design and development of continuum structure for robotic flower," in *2011 IEEE International Conference on Robotics and Biomimetics*, 2011, pp. 118–123.

[6] D. Trivedi, C. D. Rahn, W. M. Kier, and I. D. Walker, "Soft robotics: biological inspiration, state of the art, and future research," *Applied Bionics and Biomechanics*, vol. 5, no. 3, pp. 99–117, Dec. 2008.

[7] M. Russo *et al.*, "Continuum robots: an overview," *Advanced Intelligent Systems*, pp. 1–25, Mar. 2023.

[8] J. Burgner-Kars, D. Rucker, and H. Choset, "Continuum robots for medical applications: a survey," *IEEE Trans. Robot.*, pp. 1261–1280, Dec. 2015.

[9] M. W. Hannan and I. D. Walker, "Kinematics and the implementation of an elephant's trunk manipulator and other continuum style robots," *Journal of Robotic Systems*, vol. 20, no. 2, pp. 45–63, Feb. 2003.

[10] M. D. Grissom *et al.*, "Design and experimental testing of the octarm soft robot manipulator," in *Unmanned Systems Technology VIII*, vol. 6230, May 2006.

[11] I. D. Walker *et al.*, "Continuum robot arms inspired by cephalopods," in *Proceedings of SPIE Vol. 5804*, May 2005.

[12] G. Qin *et al.*, "A snake-inspired layer-driven continuum robot," *Soft Robotics*, vol. 9, no. 4, 2021.

[13] M. B. Wooten and I. D. Walker, "Vine-inspired continuum tendril robots and circumnutations," *Robotics*, vol. 7, no. 3, p. 58, 2018.

[14] M. M. Coad *et al.*, "Vine robots," *IEEE Robot. Autom. Mag.*, pp. 120–132, Sep. 2020.

[15] I. D. Walker, "Continuous backbone 'continuum' robot manipulators," *International Scholarly Research Notices*, Jul. 2013.

[16] Y. Dai, X. Chen, X. Wang, and H. Yuan, "A novel space robot with triple cable-driven continuum arms for space grasping," *Micromachines*, p. 416, 2023.

[17] E. Amanov, T.-D. Nguyen, and J. Burgner-Kahrs, "Tendon-driven continuum robots with extensible sections–a model-based evaluation of path-following motions," *The International Journal of Robotics Research*, pp. 7–23, Nov. 2019.

[18] Q. Qi *et al.*, "Design and motion control of a tendon-driven continuum robot for aerospace applications," *Proceedings of the Institution of Mechanical Engineers, Part G: Journal of Aerospace Engineering*, pp. 1296–1310, 2024.

[19] W. Zhong, Y. Huang, D. Hong, and N. Shao, "Design and control of an ultra-slender push-pull multisection continuum manipulator for in-situ inspection of aeroengine," in *2024 IEEE/RSJ International Conference on Intelligent Robots and Systems (IROS)*, 2024, pp. 11 394–11 401.

[20] J. S. Mehling, M. A. Diftler, M. Chu, and M. Valvo, "A minimally invasive tendril robot for in-space inspection," in *The First IEEE/RAS-EMBS International Conference on Biomedical Robotics and Biomechatronics*, 2006, pp. 690–695.

[21] A. Mohammad, M. Russo, Y. Fang, X. Dong, D. Axinte, and J. Kell, "An efficient follow-the-leader strategy for continuum robot navigation and coiling," pp. 7493–7500, Oct. 2021.

[22] K. Liu, Z. Sun, D. Li, C. Song, and G. Gao, "Design, kinematic modeling, and validation of a helical-coiled multi-segment flexible continuum robot," *Chinese Journal of Mechanical Engineering*, 2025.

[23] D. Matsuura, R. Shioya, H. Asada, and Y. Takeda, "An extendable continuum robot arm to deal with a confined space having discontinuous contact area," in *Mechanism Design for Robotics*, 2021, pp. 265–273.

[24] T. Kato, I. Okumura, S.-E. Song, A. J. Golby, and N. Hata, "Tendon-driven continuum robot for endoscopic surgery: preclinical development and validation of a tension propagation model," *IEEE/ASME Trans. Mechatronics*, pp. 2252–2263, Oct. 2015.

[25] M. Li, R. Kang, S. Geng, and E. Guglielmino, "Design and control of a tendon-driven continuum robot," *Transactions of the Institute of Measurement and Control*, pp. 3263–3272, Jul. 2018.

[26] J. Zhang *et al.*, "A survey on design, actuation, modeling, and control of continuum robot," *Cyborg and Bionic Systems*, Jan. 2022.

[27] X. Fu, D. Zhang, L. Mo, K. Li, and X. Zhao, "Design and analysis of soft hybrid-driven manipulator with variable stiffness and multiple motion patterns," in *2024 IEEE International Conference on Robotics and Automation (ICRA)*, 2024, pp. 2979–2985.

[28] N. P. Castledine, J. H. Boyle, and J. Kim, "Design of a modular continuum robot segment for use in a general purpose manipulator," in *2019 IEEE International Conference on Robotics and Automation (ICRA)*, 2019, pp. 4430–4435.

[29] J. Ren, L. Qi, J. Yu, H. Wang, Z. Wang, and Y. Sun, "A novel tendon-driven articulated continuum robot with stabilized self-locking joints," in *2025 IEEE International Conference on Robotics and Automation (ICRA)*, 2025, pp. 11 638–11 644.

[30] R. J. Webster and B. A. Jones, "Design and kinematic modeling of constant curvature continuum robots: a review," *The International Journal of Robotics Research*, pp. 1661–1683, Nov. 2010.

[31] B. A. Jones and I. D. Walker, "Kinematics for multisection continuum robots," *IEEE Trans. Robot. Autom.*, pp. 43–55, 2006.

[32] R. Grassmann, A. Senyk, and J. Burgner-Kahrs, "Clarke transform – a fundamental tool for continuum robotics," *arXiv preprint 2409.16501*, 2024.